^{99}Tc produced by the (^{3}He,$pn\gamma$) reaction

Ben Crowe,* Hurol Aslan,† Tim Dague, D. G. Savage,‡ Sadek Zeghib,§ F. A. Rickey, and P. C. Simms
Tandem Accelerator Laboratory, Department of Physics, Purdue University, Lafayette, Indiana 47907
(Received 24 October 1996; revised manuscript received 26 September 1997)

The nuclear structure of ^{99}Tc was studied using the ^{98}Mo(^{3}He,$pn\gamma$) reaction, which has populated most states in the nucleus below 2 MeV excitation energy. The proton exit channel was isolated from competing reaction channels by operating γ-ray detectors in coincidence with a large-solid-angle proton detector. The experiments included γ-ray excitation functions, γ-ray angular distributions, and γ-γ coincidences. The results were interpreted using a particle-rotor model. The systematics of increasing deformations in odd-*A* Tc nuclei are discussed. [S0556-2813(98)00202-7]

PACS number(s): 23.20.En, 23.20.Lv, 25.55.Hp, 27.60.+j

I. INTRODUCTION

Previous work [1–4] has shown that most states in a nucleus below 2 MeV excitation can be observed using ^{3}He fusion reactions with projectile energy a few MeV above the Coulomb barrier. Most other reactions populate some subset of the states actually present, with the result that different nuclear models can provide similar interpretations of the observed states. This paper reports our investigation of ^{99}Tc. Since we have approximately doubled the known states below 2 MeV, this experiment provides a more complete data set which can be used to evaluate competing models of transitional nuclei.

In the studies of ^{97}Tc [3] and ^{101}Tc [4] a particle-rotor model was used successfully to interpret the data. Since ^{99}Tc would be expected to have a deformation intermediate to that of the former nuclides, we have used the same model for our interpretation of the present data. The model utilizes a rotational Hamiltonian in the strong coupling limit modified to include a variable moment of inertia [5]. Pairing is treated by the BCS formalism. The Coriolis and recoil terms are treated to all order. This basic model has been used for years to interpret strongly deformed nuclei.

The ^{98}Mo(^{3}He,$pn\gamma$)^{99}Tc reaction was used in this experiment. A large-solid-angle proton detector was operated in coincidence with γ-ray detectors to separate the pn exit channel from xn and αxn channels. The measurements include γ-ray excitation functions, angular distributions, and γ-γ coincidences.

II. EXPERIMENTAL TECHNIQUES

The target was a foil of isotopically enriched ^{98}Mo rolled to a uniform thickness of 3.0 mg/cm^{2}. The composition was 97.7% ^{98}Mo with 0.5% impurities of ^{95,96,97,100}Mo. The ^{3}He beam currents of 10–25 nA were supplied by the Purdue FN Tandem Van de Graaff accelerator.

A. Excitation functions

Proton-gated singles spectra were recorded at 13.5, 15, 16.5, and 18 MeV. A typical spectrum is shown in Fig. 1. The angular distribution and γ-γ coincidence experiments were run at 18 MeV. The primary reason for this choice was to minimize competition from ^{98}Mo(^{3}He,$3n\gamma$)^{98}Ru and reactions following the breakup of ^{3}He. ^{100}Tc γ rays from the $1p$ exit channel were included in the proton-gated spectrum, but they were much weaker than the ^{99}Tc γ rays.

The angular distribution measurement consisted of proton-gated singles spectra collected at 0°, 45°, and 90° with respect to the beam line. The coincidence measurement

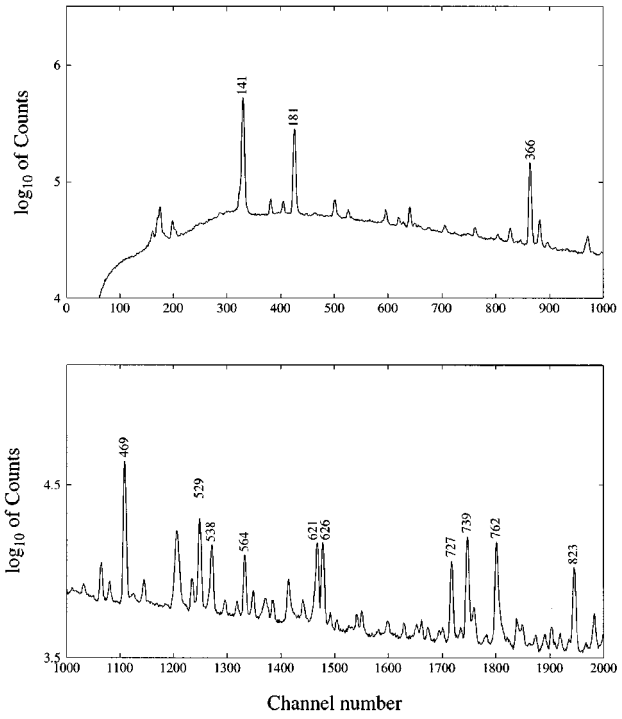

FIG. 1. A portion of a proton-gated singles spectrum from the ^{98}Mo(^{3}He,$pn\gamma$)^{99}Tc reaction at a laboratory energy of 18 MeV.

*Present address: Triangle Universities Nuclear Laboratory, Durham, NC 27706.

†Present address: Department of Nuclear Engineering, Hacettepe University, Ankara, Turkey.

‡Present address: Kinetic Systems Corporation, Lockport, IL 60441.

§Present address: Institut des Sciences Exactes et Technologie, Universite de Constantine, Constantine, Algeria.

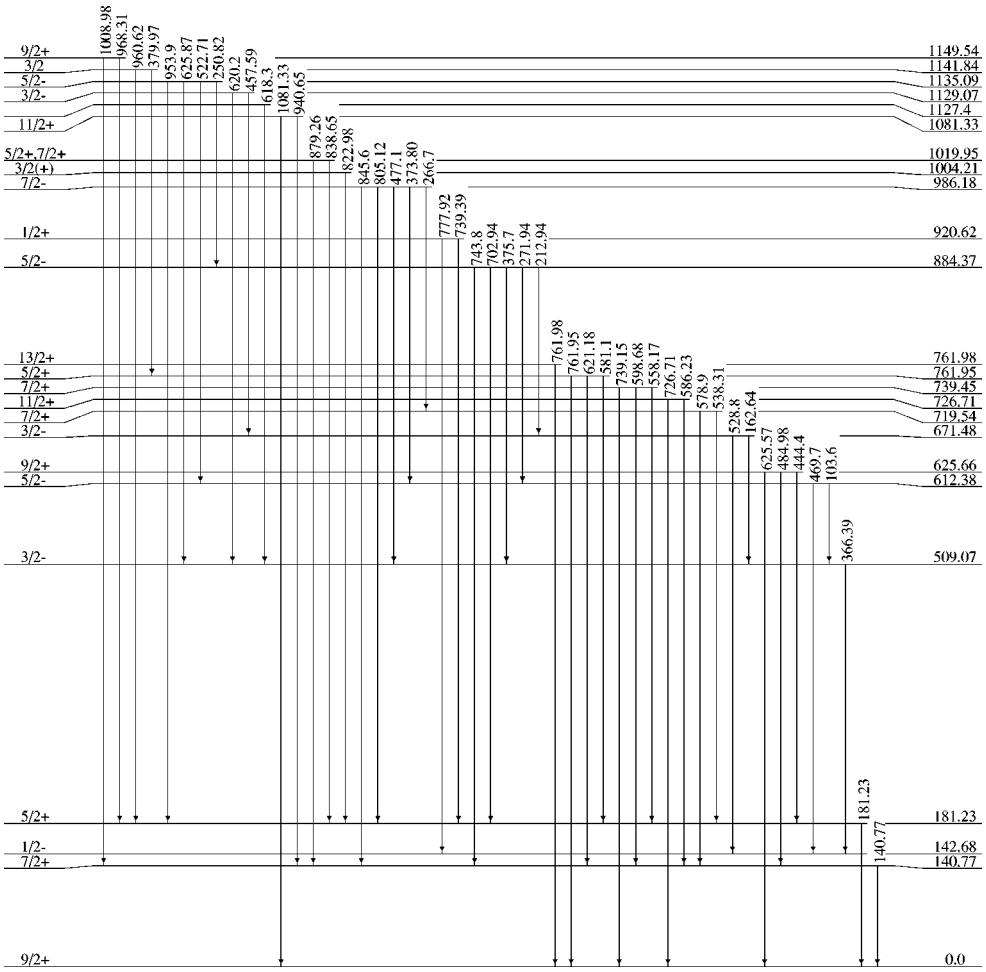

FIG. 2. The low energy portion of the level scheme deduced for ^{99}Tc. Note that the vertical energy scale is not linear.

was performed using two detectors positioned at 0° and 100° with respect to the beam axis. Additional information on these experimental techniques has been published previously [3,4].

III. THE LEVEL SCHEME

The decay scheme deduced in the present work for ^{99}Tc is shown in Figs. 2, 3, and 4. 124 γ rays were identified as belonging to ^{99}Tc and placed unambiguously in the level scheme. The level scheme contains 59 states, 29 of which are new.

A tabular form of the level scheme is given in Table I. New states are marked with a superscript *a* following their energy. Most γ rays were placed by coincidence with γ rays that precede and follow in the decay pattern. In some cases several γ rays were assigned to the same state on the basis of energy agreement, because the observed feeding to the state was too weak to provide coincidence confirmation (indicated by superscript *b* on the γ-ray energy). The precision of most γ-ray energy measurements was approximately 50 eV. Less accurate measurements are indicated by significant figures.

The spin and parity assignments are based on a combination of several sources: previous data compiled in Ref. [6], a (^{3}He,*d*) study [7], β decay measurements [8], a (^{6}Li,$3n\gamma$) study [9], γ-ray branching patterns, and our analysis of excitation functions, angular distributions, and directional correlations in the coincidence data. Many new spin assignments were made and others were confirmed that had been considered tentative in Ref. [6]. Ambiguity in spin assignment is indicated by multiple spin values. A tentative assignment is shown in parentheses.

A γ-ray excitation function depends on the angular momentum of the state from which it is emitted. The excitation functions were normalized to that of the 140.77-keV transition from a $7/2^{+}$ state to remove the common energy dependence. Then the γ-ray intensity was fitted to an exponential function of energy:

$$I_{\gamma} \propto e^{bE}. \tag{1}$$

The exponential ''slope'' *b* is approximately proportional to the angular momentum of the state. (Variations of this technique are common [10,11].)

Equal slope intervals were used to estimate the angular momentum, as listed in Table II. These slope intervals were derived from transitions depopulating states of known spin [6]. A different set of intervals was necessary for positive- and negative-parity states. The ''data used'' column in Table I has an *E* when the excitation function was used to help assign angular momentum and parity to a state.

The angular distribution data were used to restrict angular momentum and parity choices. Only the general size and

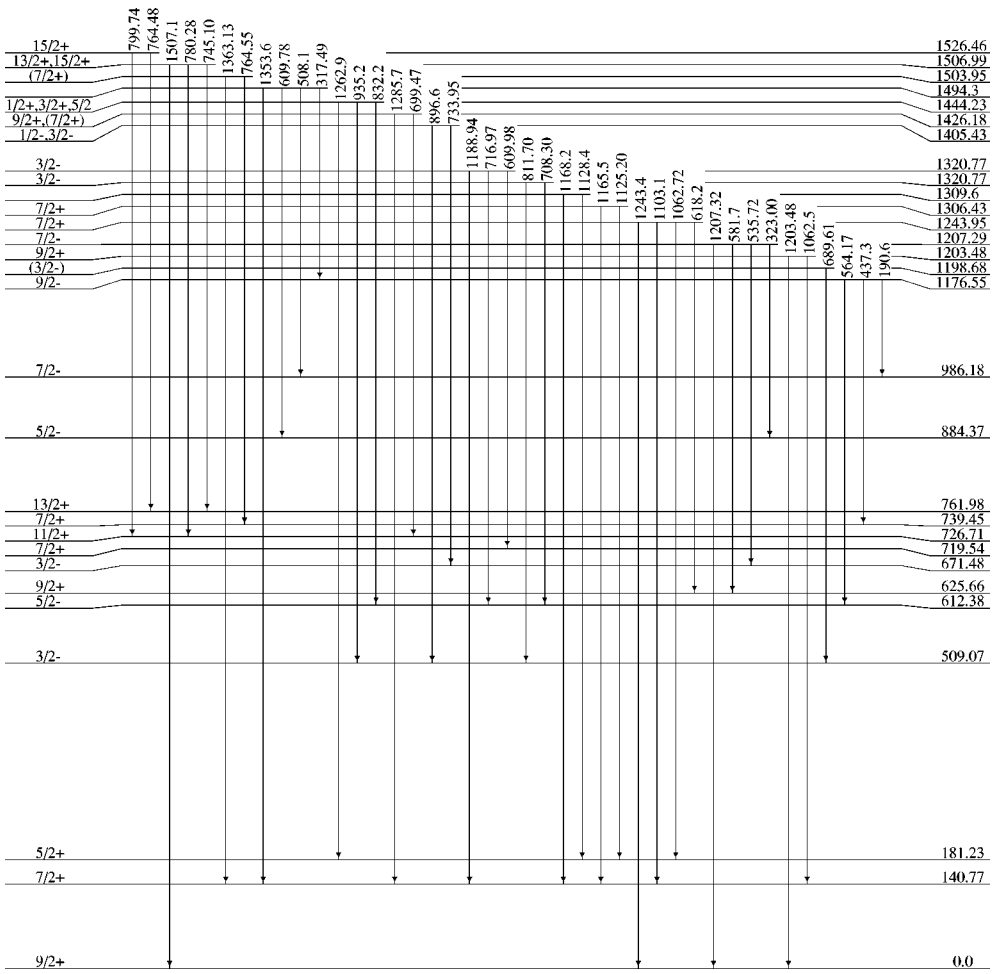

FIG. 3. The intermediate energy portion of the level scheme deduced for ^{99}Tc. The energy scale is not linear.

sign of the A_{22} was used because the degree of nuclear orientation was not well known. The measured A_{22} values are listed in Table I.

Additional angular momentum information was obtained from DCO analysis [12,13] of the coincidence data. (DCO stands for γ-γ directional correlation from oriented nuclei.) The DCO was used whenever there was substantial interference between γ rays or the uncertainty from the DCO was smaller than from the angular distribution. Complete DCO analysis [12] was performed but the DCO ratio was not given in Table I. Instead, we have calculated the value of A_{22} that the γ ray would have for the spin sequence and mixing ratio required by the experimental DCO ratio. Then the angular distribution and DCO measurements can be evaluated on the same basis. These ''implied'' A_{22} values are listed in Table I. The ''data-used'' column of Table I tells when the angular distribution (A) or DCO (D) was used in the spin analysis. A subscript π is added to A or D when the measurement does not allow parity change for the γ transition.

The γ-ray intensity was taken from the angular distribution measurement, unless the coincidence analysis showed that there was a second γ ray unresolved from the γ ray of interest. In that case, the intensity was taken from the coincidence analysis.

An N in the data-used column indicates that the Ref. [6] spin and parity assignment was used. Our measurements were consistent with that assignment but added little new information. The numbers in the data-used column are references to previous work that was used in our spin and parity assignment. Most of the data from these references also is found in Ref. [6].

The 1329.52-keV state in our decay scheme, which emits 609.98- and 1188.94-keV γ rays is inconsistent with Zell *et al.* [9], who report separate states at 1329.13 and 1329.8 keV that emit 1188.6- and 610.1-keV γ rays, respectively. The energy of our state that emits the 1188.94-keV γ ray would be 1329.35 keV, which is too close (170 eV) in energy to suggest a state separate from the 1329.52-keV state. Furthermore, they report that the 1329.13-keV state emits a 247.5-keV γ ray that we do not observe, and we observe a 716.97-keV γ ray from the 1329.52-keV state that they do not report.

IV. DISCUSSION AND INTERPRETATION

In recent years both interacting boson fermion (IBFM) [14] and rotational [2–4] models have been used to interpret collective structure in odd-A mass 100 nuclei. An IBFM calculation for the interpretation of ^{99}Tc was presented in previous work [9]. The calculation reproduced the energies of positive-parity yrast states very nicely. For other positive-parity states the energy agreement was not as good, and

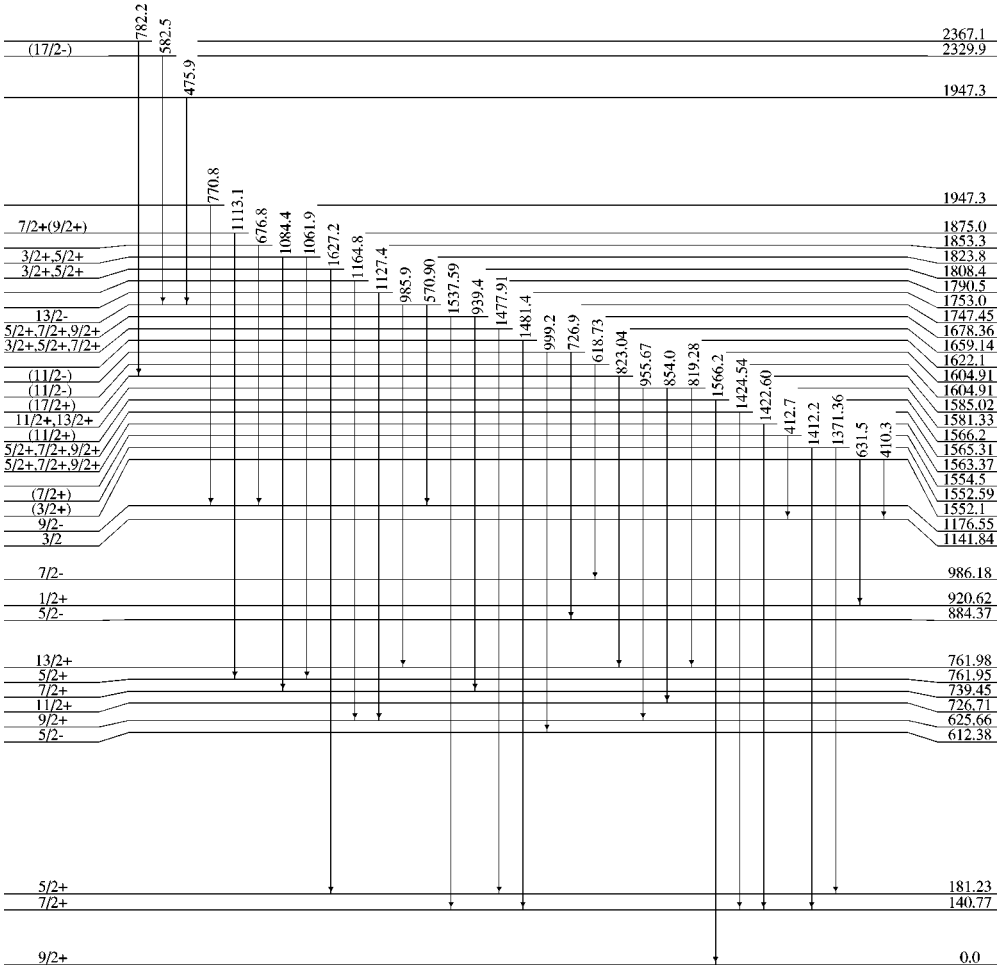

FIG. 4. The higher energy portion of the level scheme deduced for ^{99}Tc. The energy scale is not linear.

without transition probability calculations the associations were not very conclusive. No results for negative-parity states were presented. In ^{97}Tc [3] and ^{101}Tc [4] rotational calculations at deformations of $\delta=0.24$ and $\delta=0.28$ successfully interpreted the observed structure. For these reasons the use of a rotational model for the interpretation of the structure observed in ^{99}Tc seemed reasonable. A deformation of $\delta=0.26$ is intermediate to those used in ^{97}Tc and ^{101}Tc, and gave the best results. In the comparison of the results of the calculation to the experimental results, emphasis has been placed on electromagnetic decay properties.

The rotational model used was a symmetric particle-plus rotor model, which has been described previously. The basic model has been used for years to interpret strongly deformed nuclei. The calculation of energies and wave functions was the same as that used by Smith and Rickey [5] for Pd nuclei. The calculation of electromagnetic transition properties was the same as that used by Popli [16] for Ag nuclei. This specific model utilizes a rotational Hamiltonian in the strong-coupling limit, modified to include a variable moment of inertia (VMI) [17]. The basis states are thus rotational states built on Nilsson single-particle states [15], characterized by good K and Ω, the projections of the total angular momentum $\vec{I}$ and the particle angular momentum $\vec{j}$, respectively, on the symmetry axis. Pairing is treated by the BCS formalism. The Coriolis and recoil terms, which mix these states, are treated to all order. Aside from differences in inertial quantities, the only deviations of its predictions from familiar rotational patterns are due to the role of the Coriolis interaction.

The parameters used for the Nilsson calculations were chosen to give energies at zero deformation consistent with those tabulated by Reehal and Sorenson [18], and are the same as those used for ^{97}Tc and ^{101}Tc. The Nilsson diagram appropriate for odd protons in ^{99}Tc is shown in Fig. 5. The Fermi energies for positive and negative parities were first estimated based on the 43 protons of ^{99}Tc, and then adjusted to give the best fits to the experimental states. The pairing parameter Δ, and Coriolis and recoil attenuations, were taken from systematics. The values of these parameters are given in Table III.

The basis states for the calculation were restricted to the Nilsson states near the Fermi surface. The specific states included in the basis, along with their single-particle energies, are given in Table IV. The VMI parameters are also given in Table IV. Energies of basis states are affected by the use of a VMI. Consider the $5/2^{+}[422]$ band, which from an inspection of the Nilsson diagram of Fig. 5 would be expected near the Fermi surface. If a fixed moment-of-inertia had been used, the rotational energies would follow a simple $I(I+1)$ pattern. This is illustrated in the left part of Fig. 6. The VMI systematically suppresses the energies of high-spin states

TABLE I. Analysis of γ-rays emitted following the ^{98}Mo(^{3}He,pn)^{99}Tc reaction at 18 MeV.

E_i (keV)	I_i^π	E_γ (keV)	I_f^π	E_f (keV)	Intensities ^{99}Tc	Intensities other	A_{22} ×100	Exc. func.	Data used[d]
140.77	$\frac{7}{2}^+$	140.77	$\frac{9}{2}^+$	0	1000		2(3)	0(2)	N
142.68	$\frac{1}{2}^-$	142.68	$\frac{9}{2}^+$	0					N
181.23	$\frac{5}{2}^+$	181.23	$\frac{9}{2}^+$	0	477		10(2)	-25(1)	N
509.07	$\frac{3}{2}^-$	366.39	$\frac{1}{2}^-$	142.68	339		1(2)	-2(1)	E,A,A_π
612.38	$\frac{5}{2}^-$	469.70	$\frac{1}{2}^-$	142.68	451		20(2)	56(1)	E,A,A_π
		103.6	$\frac{3}{2}^-$	509.07	7				
625.66	$\frac{9}{2}^+$	625.57	$\frac{9}{2}^+$	0	151	14	23(2)	70(1)	E,A
		484.98	$\frac{7}{2}^+$	140.77	30		36(7)	124(6)	E,A,A_π
		444.4	$\frac{5}{2}^+$	181.23	3				
671.48	$\frac{3}{2}^-$	528.80	$\frac{1}{2}^-$	142.68	187		6(2)	13(1)	E,A,A_π
		162.64	$\frac{3}{2}^-$	509.07	42		9(5)	-11(1)	E,A
719.54	$\frac{7}{2}^+$	538.31	$\frac{5}{2}^+$	181.23	119		18(2)	31(2)	E,A,A_π, [7]
		578.9	$\frac{7}{2}^+$	140.77	8	17	0(11)		D_π
726.71	$\frac{11}{2}^+$	726.71	$\frac{9}{2}^+$	0	164		46(2)	160(2)	E,A_π
		586.23	$\frac{7}{2}^+$	140.77	23		40(6)	157 (12)	E,A_π, [9]
739.45[a]	$\frac{7}{2}^+$	739.15	$\frac{9}{2}^+$	0	148	71			
		598.68	$\frac{7}{2}^+$	140.77	50		5(4)	6(3)	E,A_π
		558.17	$\frac{5}{2}^+$	181.23	16		-10(9)	-16(3)	E,D
761.95	$\frac{5}{2}^+$	621.18	$\frac{7}{2}^+$	140.77	145		0.5(2)	-42(1)	E,A_π, [8]
		761.98	$\frac{9}{2}^+$	0	32	198			
		581.1	$\frac{5}{2}^+$	181.23	17	8	-6(8)		D_π
761.98	$\frac{13}{2}^+$	761.98	$\frac{9}{2}^+$	0	198	32	31(2)	217(2)	E,A,A_π
884.37[a]	$\frac{5}{2}^-$	271.94	$\frac{5}{2}^-$	612.38	51		13(3)	70(3)	E,A
		212.94	$\frac{3}{2}^-$	671.48	44		0(3)	26(4)	E,A_π
		702.94	$\frac{5}{2}^+$	181.23	21		14(5)		A
		743.8	$\frac{7}{2}^+$	140.77	22	13	-6(7)		D
		375.7	$\frac{3}{2}^-$	509.07	4				
920.62	$\frac{1}{2}^+$	739.39	$\frac{5}{2}^+$	181.23	71	148			N
		777.92	$\frac{1}{2}^-$	142.68	33				
986.18	$\frac{7}{2}^-$	373.80	$\frac{5}{2}^-$	612.38	54		-17(3)	91(5)	E,A
		805.12	$\frac{5}{2}^+$	181.23	22		-18(5)		D
		845.6	$\frac{7}{2}^+$	140.77	10	10			
		266.7	$\frac{7}{2}^+$	719.54	9				
		477.1	$\frac{3}{2}^-$	509.07	8				
1004.21	$\frac{3}{2}^{(+)}$	822.98	$\frac{5}{2}^+$	181.23	113	37	-3(3)	-13(1)	E,D
1019.95[a]	$\frac{5}{2}^+$,$\frac{7}{2}^+$	879.26	$\frac{7}{2}^+$	140.77	76		4(4)	-26(4)	E,A_π
		838.65[b]	$\frac{5}{2}^+$	181.23	51		10(4)	-20(4)	E,A_π
1081.33	$\frac{11}{2}^+$	1081.33	$\frac{9}{2}^+$	0	50		-41(5)	140(5)	E,A,A_π
		940.65[b]	$\frac{7}{2}^+$	140.77	29		22(4)		A,A_π
1127.4[a]		618.3	$\frac{3}{2}^-$	509.07	7	33			
1129.07	$\frac{3}{2}^-$	457.59	$\frac{3}{2}^-$	671.48	23		9(5)	15(2)	E,A, [8]
		620.2[b]	$\frac{3}{2}^-$	509.07	7	145			
1135.09[a]	$\frac{5}{2}^-$	522.71	$\frac{5}{2}^-$	612.38	40		-13(3)	63(4)	E,A_π
		250.82[b]	$\frac{5}{2}^-$	884.37	8				
		625.87[b]	$\frac{3}{2}^-$	509.07	14	151			
		953.9[b]	$\frac{5}{2}^+$	181.23	10	5	21(15)		D
1141.84	$\frac{3}{2}$	960.62	$\frac{5}{2}^+$	181.23	84		5(6)	-44(8)	[8]
		379.97	$\frac{5}{2}^+$	761.95	10		-2(5)		
1149.54	$\frac{9}{2}^+$	968.31	$\frac{5}{2}^+$	181.23	33		26(5)	105(10)	E,A,A_π
		1008.98[b]	$\frac{7}{2}^+$	140.77	30	9	-29(4)	107(5)	E,A
1176.55	$\frac{9}{2}^-$	564.17	$\frac{5}{2}^-$	612.38	107		29(3)	165(1)	E,A,A_π
		437.15	$\frac{7}{2}^+$	739.45	13		-10(6)		A
		190.6	$\frac{7}{2}^-$	986.18	4	3			

TABLE I. (*Continued*).

E_i (keV)	I_i^π	E_γ (keV)	I_f^π	E_f (keV)	Intensities ^{99}Tc	Intensities other	A_{22} ×100	Exc. func.	Data used[d]
1198.68	$(\frac{3}{2}^-)$	689.61	$\frac{3}{2}^-$	509.07	15		10(4)	-30(6)	*E*,*D*
1203.48[a]	$\frac{9}{2}^+$	1203.48	$\frac{9}{2}^+$	0	15		22(9)	83(24)	*E*,*A*
		1062.5[b]	$\frac{7}{2}^+$	140.77	37	33	-1(5)		*D*
1207.29[a]	$\frac{7}{2}^-$	323.00	$\frac{5}{2}^-$	884.37	21		23(10)	40(13)	A_π
		535.72[b]	$\frac{3}{2}^-$	671.48	19		19(8)	36(14)	*A*,A_π
		1026.14[b]	$\frac{5}{2}^+$	181.23	14		-10(7)		*A*
		1207.32[c]	$\frac{9}{2}^+$	0	13				
		581.7[b]	$\frac{9}{2}^+$	625.66	4				
1243.95[a]	$\frac{7}{2}^+$	1062.72	$\frac{5}{2}^+$	181.23	30	40	-14(2)		*D*
		1103.1[b]	$\frac{7}{2}^+$	140.77	6	4			
		1243.4[c]	$\frac{9}{2}^+$	0	17			17(22)	*E*
		618.2[b]	$\frac{9}{2}^+$	625.66	4	36			
1306.43[a]	$\frac{7}{2}^+$	1125.20	$\frac{5}{2}^+$	181.23	32		-14(8)	29(14)	*E*,*A*
		1165.5[b]	$\frac{7}{2}^+$	140.77	7	7	24(9)		*D*
1309.6[a]		1128.4	$\frac{5}{2}^+$	181.23	9	9			
		1168.2[b]	$\frac{7}{2}^+$	140.77	6				
1320.77[a]	$\frac{3}{2}^-$	811.70	$\frac{3}{2}^-$	509.07	16		14(6)	-3(10)	*E*,*A*
		708.30[b]	$\frac{5}{2}^-$	612.38	11				
1329.52[a]	$\frac{7}{2}^-$	609.98	$\frac{7}{2}^+$	719.54	15	20	13(6)		*D*
		716.97[b]	$\frac{5}{2}^-$	612.38	14		21(10)	35(12)	*A*,A_π
		1188.94[b]	$\frac{7}{2}^+$	140.77	15	5	24(10)	101(8)	*E*
1405.43[a]	$\frac{1}{2}^-,\frac{3}{2}^-$	733.95	$\frac{3}{2}^-$	671.48	15			-56(7)	*E*
		896.6[b]	$\frac{3}{2}^-$	509.07	6				
1426.18[a]	$\frac{9}{2}^+,(\frac{7}{2}^+)$	699.47	$\frac{11}{2}^+$	726.71	15		9(9)	38(14)	*E*,*D*
		1285.7[b]	$\frac{7}{2}^+$	140.77	14		-29(17)		*A*
1444.23[a]	$\frac{1}{2}^+,\frac{3}{2}^+,\frac{5}{2}$	1262.99	$\frac{5}{2}^+$	181.23	13	4	17(14)		D_π
		935.2[b]	$\frac{3}{2}^-$	509.07	6	5			
		832.2[b]	$\frac{5}{2}^-$	612.38	5	4			
1494.3[a]		1353.6	$\frac{7}{2}^+$	140.77	7	5			
		609.8[b]	$\frac{5}{2}^-$	884.37	6	29			
		508.1[b]	$\frac{7}{2}^-$	986.18	4				
1503.95[a]	$(\frac{7}{2}^+)$	764.55	$\frac{7}{2}^+$	739.45	15	32	5(9)		D_π
		1363.13[b]	$\frac{7}{2}^+$	140.77	12	4	4(11)	16(7)	*E*,A_π
1506.99	$\frac{13}{2}^+,(\frac{15}{2}^+)$	780.28	$\frac{11}{2}^+$	726.71	15	3	29(14)		D_π
		745.10[b]	$\frac{13}{2}^+$	761.98	13	29	34(17)		D_π, [9]
		1507.1[c]	$\frac{9}{2}^+$	0	11				
1526.46	$\frac{15}{2}^+$	764.48	$\frac{13}{2}^+$	761.98	32	15	32(10)		D_π
		799.74[b]	$\frac{11}{2}^+$	726.71	16		32(10)	324(5)	*E*,*A*,A_π
1552.1[a]	$(\frac{3}{2}^+)$	631.5	$\frac{1}{2}^+$	920.62	11	5	-15(5)		*D*
		410.3[b]	$\frac{3}{2}^+$	1141.84	6	9	10(10)		*D*
1552.59[a]	$(\frac{7}{2}^+)$	1371.36	$\frac{5}{2}^+$	181.23	20		0(7)	4(11)	*E*,A_π
		1412.2[b]	$\frac{7}{2}^+$	140.77	12			37(23)	*E*
1554.5[a]		412.7	$\frac{3}{2}^+$	1141.83	6	36			
1563.37[a]	$\frac{5}{2}^+,\frac{7}{2}^+,\frac{9}{2}^+$	1422.60	$\frac{7}{2}^+$	140.77	11	17	-37(12)		*D*
1565.31[a]	$\frac{5}{2}^+,\frac{7}{2}^+,\frac{9}{2}^+$	1424.54	$\frac{7}{2}^+$	140.77	11		-21(11)		*D*
1566.2[a]	$(\frac{11}{2}^+)$	1566.2	$\frac{9}{2}^+$	0	17		-34(10)		*A*
1581.33[a]	$\frac{11}{2}^+,\frac{13}{2}^+$	955.67	$\frac{9}{2}^+$	625.66	14		42(22)		A_π
		819.28[b]	$\frac{13}{2}^+$	761.98	10	4	-27(13)		D_π
		854.0[b]	$\frac{11}{2}^+$	726.71	3				
1585.02	$(\frac{17}{2}^+)$	823.04	$\frac{13}{2}^+$	761.98	37	113	31(5)		*D*,D_π
1604.91	$(\frac{11}{2}^-)$	618.73	$\frac{7}{2}^-$	986.18	21	19	30(7)		*D*,D_π

TABLE I. (*Continued*).

E_i (keV)	I_i^π	E_γ (keV)	I_f^π	E_f (keV)	Intensities ^{99}Tc	Intensities other	A_{22} ×100	Exc. func.	Data used[d]
1611.5[a]	$\frac{1}{2}-,\frac{3}{2}-,\frac{5}{2}-$	999.2	$\frac{5}{2}-$	612.38	8		10(18)		*A*
		726.9[b]	$\frac{5}{2}-$	884.37	5	164			
1622.1[a]		1481.4	$\frac{7}{2}+$	140.77	9	7			
1659.14[a]	$\frac{3}{2}+,\frac{5}{2}+,\frac{7}{2}+$	1477.91	$\frac{5}{2}+$	181.23	17		-13(13)	-48(16)	*E*,*D*
1678.36[a]	$\frac{5}{2}+,\frac{7}{2}+,\frac{9}{2}+$	1537.59	$\frac{7}{2}+$	140.77	11	5	-7(21)		*D*
		939.4[b]	$\frac{7}{2}+$	739.42	5	29			
1747.45	$\frac{13}{2}-$	570.90	$\frac{9}{2}-$	1176.55	39		37(5)	308(2)	E,A,A_π
		985.9[b]	$\frac{13}{2}+$	761.98	6	4			
1753.0[a]		1127.4	$\frac{9}{2}+$	625.66	8	9			
1790.5[a]		1164.8	$\frac{9}{2}+$	625.66	8	7			
1808.4[a]	$\frac{3}{2}+,\frac{5}{2}+$	1627.2	$\frac{5}{2}+$	181.23	11			-103(15)	*E*
1823.8[a]	$\frac{3}{2}+,\frac{5}{2}+$	1084.4	$\frac{7}{2}+$	739.45	9			-139(6)	*E*
		1061.9[b]	$\frac{5}{2}+$	761.95	8	62			
1853.3[a]		676.8	$\frac{9}{2}-$	1176.55	9	7			
1875.0[a]		1113.1	$\frac{5}{2}+$	761.95	8				
1947.3[a]		770.8	$\frac{9}{2}-$	1176.55	5	6			
2329.9		582.5	$\frac{13}{2}-$	1747.45	7				
2367.1[a]		782.2	$\frac{15}{2}+$	1585.02	8	14			

[a]New states observed in this experiment.
[b]Placed in ^{97}Tc by coincidence with following γ rays, but assigned to this state on the basis of energy agreement.
[c]Placed between known states by energy agreement alone.
[d]*N* means that the NDS [6] spin and parity assignment was used. *E*, *A*, or *D* mean that the excitation function, angular distribution, or DCO, respectively, was used in the spin and parity assignment. A subscript π is added to *A* or *D* when the measurement excludes parity change for the γ transition.

relative to lower-spin states. This effect is shown in the center portion of Fig. 6. A similar situation exists for all other bands in the basis.

Table V presents the comparison of experimental and calculated results for ^{99}Tc. This table includes only the experimental states which have been identified on the basis of their energies and branching ratios as corresponding to rotational states predicted by the model. Columns 1 and 2 give the experimental and theoretical energies for each initial state, and column 3 gives the initial spin and parity. If more than one spin was experimentally possible, only the spin agreeing with the theoretical spin is listed and identified with a footnote. (There are two states in this category.) The model identification of the initial state is given in column 8. In the calculation we considered decay probabilities to all final states to which transitions were possible on the basis of energies and spin changes. However, because of space limitations, the table only includes branches which were either observed or predicted to be observable. For the branches included, column 4 gives the final spin and parity and column 5 the γ-ray energy. Columns 6 and 7 give the experimental and theoretical branching ratios, and column 9 gives the model identification for each final state.

TABLE II. Excitation function slope intervals for spin assignment.

	Slope interval			
	Positive parity		Negative parity	
Spin	Min.	Max.	Min.	Max.
$\frac{1}{2}$		−153		−46
$\frac{3}{2}$	−153	−81	−46	+16
$\frac{5}{2}$	−81	−8	+16	+78
$\frac{7}{2}$	−8	+64	+78	+140
$\frac{9}{2}$	+64	+136	+140	+199
$\frac{11}{2}$	+136	+208	+199	+263
$\frac{13}{2}$	+208	+281	+263	+325
$\frac{15}{2}$	+281	+353	+325	+387
$\frac{17}{2}$	+353		+387	

When Coriolis mixing is large, the odd particle tends to become decoupled from the core, and *j* and *R*, the angular momentum of the core, become better quantum numbers than *K* and Ω. This limit can be approached, even at relatively high deformations, when *j* is large. In Tc nuclei, this may be the case for states of predominantly $g_{9/2}$ parentage. The model associates a group of positive-parity states included in Table V with Nilsson states of predominantly $g_{9/2}$ parentage. Because of the larger Coriolis mixing, Ω is not a good quantum number. However, there is a trend for one Nilsson component to be larger than the others for many of the states, which is a clear sign of the substantial deformation of ^{99}Tc. For example, the lowest $5/2^+$, $7/2^+$, $9/2^+$, and $11/2^+$ states have a large $5/2^+[422]$ component. The result is

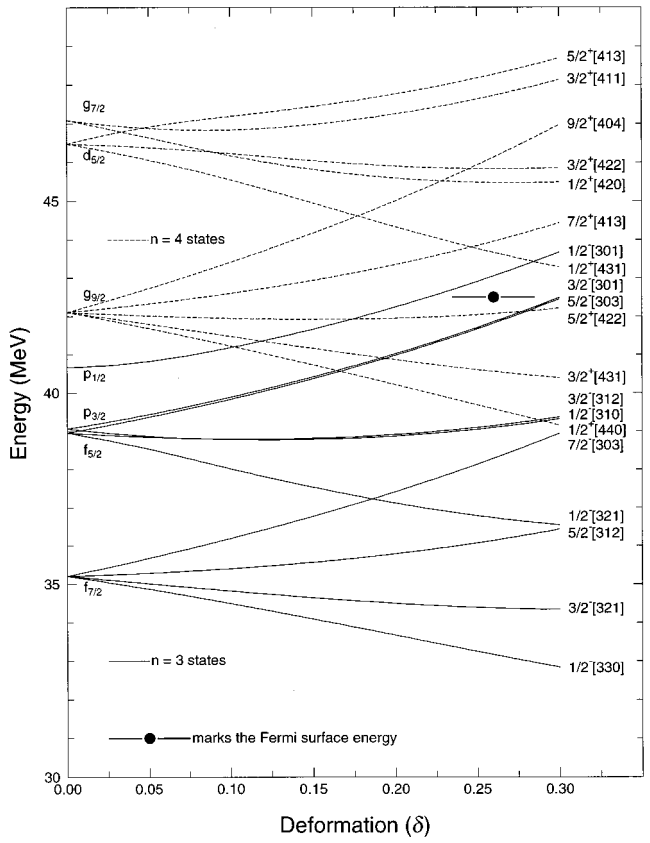

FIG. 5. Nilsson diagram for odd protons in ^{99}Tc.

a ''quasi'' $5/2^+[422]$ band, but with scrambled energies at the lower spins. The calculation for this group of states is shown in the right part of Fig. 6. In addition, most of the wave functions contain more than one sizable value of R. Even the $9/2^+$ ground state, which should be a pure $R=0$ state when the deformation is small, shows a large component of $R=2$. In the identification column of Table V, more than one R component is listed if the dominant R component was less than 0.8.

When Coriolis mixing is small, the model predicts relatively pure Nilsson bands, although energies may depart from the familiar spacings observed in rare-earth or actinide nuclei. This limit is approached not only when the deformation is high, but when low values of $\vec{j}$ are involved, or when $j \approx \Omega$.

An inspection of the Nilsson diagram of Fig. 5 shows that $1/2^-[301]$, $3/2^-[301]$, and $5/2^-[303]$ Nilsson states are expected near the Fermi surface. Three negative-parity ''bands'' have been identified, with bandheads $1/2^-$, $3/2^-$, and $5/2^-$. These three bands, along with the predicted energies, are shown in Fig. 7. The calculated wave functions for members of the $1/2^-$ band are better than 90% $1/2^-[301]$, so

TABLE III. Parameters used in the calculation.

Shell number	κ	μ	μ_2	λ (MeV)	Δ (MeV)	Atten. factor
4	0.062	0.45	0.43	41.70	1.5	0.95
3	0.060	0.52	0.52	42.70	1.5	0.8

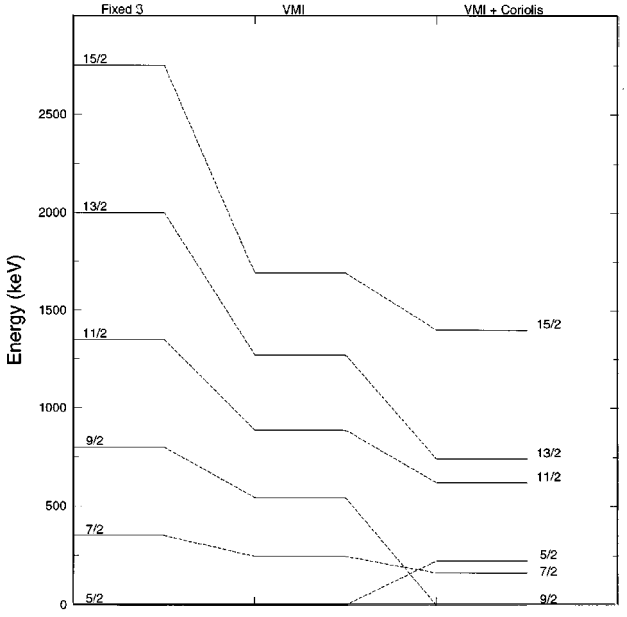

FIG. 6. The effects of including a variable moment-of-inertia and Coriolis mixing on the energy levels in a $5/2^+$ band.

that the result is an essentially pure Nilsson band. The Coriolis interaction has caused some mixing for the $3/2^-$ and $5/2^-$ bands, although it is relatively small. Members of the $3/2^-$ band are better than 85% $3/2^-[301]$, and members of the $5/2^-$ band are better than 87% $5/2^-[303]$. Thus Table V identifies the bands as $1/2^-[301]$, $3/2^-[301]$, and $5/2^-[303]$, respectively. However, this Coriolis mixing has affected transition probabilities, as will be discussed later.

As Fig. 5 shows, at deformations greater than $\delta+0.18$, the $Z=50$ shell closure disappears, and the $1/2+[431]$ Nilsson state approaches the Fermi surface. In Table V four members of a positive-parity band with a bandhead spin of $1/2^+$ have also been identified. The calculation associates this band with a relatively pure $1/2^+[431]$ Nilsson band, ranging from 63 to 83 % depending on the spin. This band, along with predicted energies, is also shown in Fig. 7. The fact that the bandhead decays by an $E1$ branch to the 142.68-keV $1/2^-$ state is a good indication of the $1/2^+[431]$ nature of the band. The $1/2^-$ state must have $p_{1/2}$ or $p_{3/2}$ parentage. The

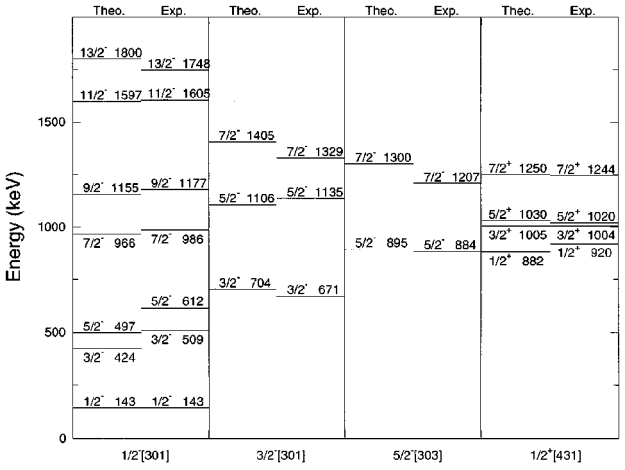

FIG. 7. Band structure identified in ^{99}Tc.

$E1$ decay is inconsistent with any state of $g_{9/2}$ parentage. The $1/2^+[431]$ Nilsson state has sizable components of $s_{1/2}$, $d_{3/2}$, and $d_{5/2}$ parentage, and the $E1$ decay is allowed. The model prediction of the $E1$ branch is too large, but $E1$ calculations are extremely sensitive to small admixtures in the wave functions. The increase in Coriolis mixing over that for the negative-parity bands is due to components of higher values of j in the wave functions.

There are of course observed states which are not described by this simple particle-rotor model. If one considers ^{98}Mo as the ''core'' for ^{99}Tc, there are three ''nonrotational'' excited states known [19] below 1.8 MeV, 0^+ (735 keV), 2^+ (1432 keV), and 2^+ (1758 keV). Thus one should expect to find ''nonrotational'' states in ^{99}Tc which are outside of the model space. Nevertheless, the model does a good job at low excitation energies. Of the 16 observed states below 1.0 MeV, 12 are accounted for by the model. As the excitation energy increases, there are more unexplained states. Between 1.0 and 1.5 MeV, 11 of the 21 observed states cannot be identified, and likewise for 19 of the 24 observed states between 1.5 and 2.0 MeV.

V. SYSTEMATICS

Technetium nuclei span a transition region from the 50-neutron closed shell (^{93}Tc) to a potential region of deformation in heavier Tc nuclei. In this perspective, changes in properties of odd-Z nuclei might be readily understood on the basis of a change in deformation only. This section discusses systematic trends which are consistent with the deformation increasing from ^{95}Tc to ^{103}Tc.

Complete rotational interpretations have been presented for ^{97}Tc and ^{101}Tc in previous work [3,4], as well as that of the present work for ^{99}Tc. We feel that there are systematic features which exhibit a picture independent of the details of the calculation. In the particle-rotor model we have used, aside from the obvious changes in inertial parameters, the dominant effects of deformation are the Nilsson states near the Fermi surface and the effects of the Coriolis interaction.

Low-lying $1/2^+$ states have been observed in ^{97}Tc [3], the present work, ^{101}Tc [4], and possibly in ^{95}Tc [20]. The energies of these states are difficult to understand without invoking some sort of collective motion. A shell model calculation for ^{93}Tc, using the computer code OXBASH [21], predicts the lowest $1/2^+$ state at 3386 keV. (No experimental $1/2^+$ state has been reported in ^{93}Tc.) The lowest known $1/2^+$ states in ^{97}Tc, ^{99}Tc, and ^{101}Tc lie at 940, 920, and 606 keV, respectively. The data for ^{95}Tc [20] are not very complete, but the lowest candidates are at 1034 (no parity assigned) or 1930 keV. No experimental $1/2^+$ state has been reported in ^{103}Tc [22]. The excitation energies of these $1/2^+$ states are not only low, but clearly decrease with increasing N. Figure 5 shows that this is consistent with increasing deformation, as the $1/2^+[431]$ Nilsson state approaches the Fermi surface.

The other Nilsson states expected near the Fermi surface for deformations of $\delta \simeq 0.18$ or higher are the negative-parity $1/2^-[301]$, $3/2^-[301]$, and $5/2^-[303]$ states, and the positive-parity $5/2^+[422]$ state. In the simplest rotational picture one might expect to observe bands built on these states, but the Coriolis interaction mixes states in these bands. However, the effects of the Coriolis interaction decrease with increasing deformation, so systematic trends should be observable.

TABLE IV. Basis states and associated parameters used in the calculation.

State	E_{sp}	$\Im_0$	C
$\frac{1}{2}^+[420]$	45.167	0.05	0.100
$\frac{1}{2}^+[431]$	43.500	0.05	0.100
$\frac{1}{2}^+[440]$	39.310	0.05	0.100
$\frac{3}{2}^+[411]$	47.401	0.05	0.100
$\frac{3}{2}^+[422]$	45.522	0.05	0.100
$\frac{3}{2}^+[431]$	40.284	0.05	0.100
$\frac{5}{2}^+[413]$	47.942	0.05	0.100
$\frac{5}{2}^+[422]$	41.783	0.05	0.200
$\frac{7}{2}^+[413]$	43.654	0.05	0.200
$\frac{9}{2}^+[404]$	45.818	0.05	0.100
$\frac{1}{2}^-[301]$	42.760	0.5	0.007
$\frac{1}{2}^-[310]$	38.828	1.0	0.003
$\frac{1}{2}^-[321]$	36.478	1.0	0.003
$\frac{3}{2}^-[301]$	41.722	1.0	0.007
$\frac{3}{2}^-[312]$	38.876	1.0	0.003
$\frac{5}{2}^-[303]$	41.535	1.0	0.003
$\frac{5}{2}^-[312]$	35.893	1.0	0.003

Although low-lying negative-parity states have been reported in ^{95}Tc [20] and ^{103}Tc [22], the data are not complete enough to examine systematic band structure. However, the expected bands are observed in ^{97}Tc, ^{99}Tc, and ^{101}Tc. The comparison of interband and intraband $M1$ decay patterns shows systematic evidence for increasing deformation as a

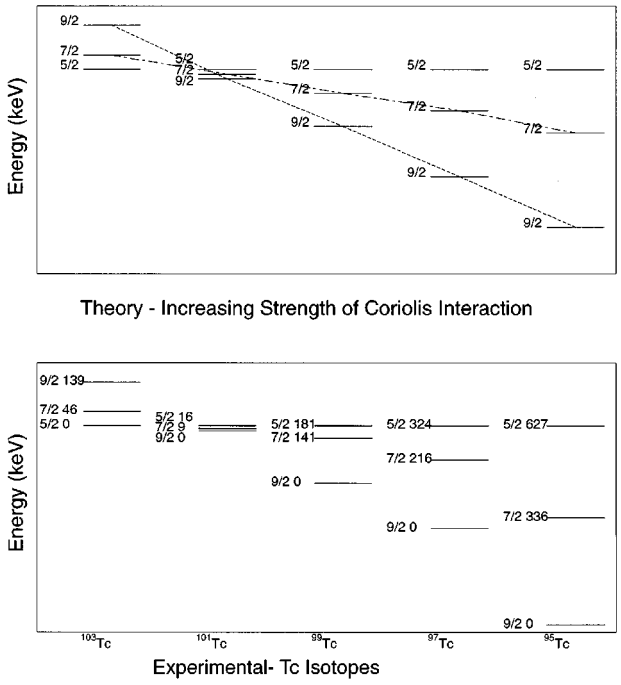

FIG. 8. A comparison of theoretical energies, as a function of the strength of the Coriolis interaction, of the three lowest-lying positive-parity states in odd-Z Tc isotopes to experimental energies.

TABLE V. Comparison of experimental and calculated results for ^{99}Tc.

E_i (keV)		I_i^π	I_f^π	E_γ (keV)	Branching ratio		Theoretical identification	
Expt.	Theor.				Expt.	Theor.	Initial state	Final state
0	0	$\frac{9}{2}^+$					$g_{9/2}, R=0,2$	
140.77	163	$\frac{7}{2}^+$	$\frac{9}{2}^+$	140.77	1.00	1.00	$g_{9/2}, R=2$	$g_{9/2}, R=0,2$
142.68	143	$\frac{1}{2}^-$	$\frac{9}{2}^+$	142.68	1.00	1.00	$\frac{1}{2}^-[301]$	$g_{9/2}, R=0,2$
181.23	224	$\frac{5}{2}^+$	$\frac{9}{2}^+$	181.23	1.00	0.77	$g_{9/2}, R=2,4$	$g_{9/2}, R=0,2$
			$\frac{7}{2}^+$	40.5	0.00	0.23		$g_{9/2}, R=2$
509.07	424	$\frac{3}{2}^-$	$\frac{1}{2}^-$	366.39	1.00	1.00	$\frac{1}{2}^-[301]$	$\frac{1}{2}^-[301]$
612.38	497	$\frac{5}{2}^-$	$\frac{1}{2}^-$	469.70	0.98	0.94	$\frac{1}{2}^-[301]$	$\frac{1}{2}^-[301]$
			$\frac{3}{2}^-$	103.6	0.02	0.06		$\frac{1}{2}^-[301]$
671.48	704	$\frac{3}{2}^-$	$\frac{1}{2}^-$	528.80	0.82	0.94	$\frac{3}{2}^-[301]$	$\frac{1}{2}^-[301]$
			$\frac{3}{2}^-$	162.64	0.18	0.06		$\frac{1}{2}^-[301]$
726.71	720	$\frac{11}{2}^+$	$\frac{9}{2}^+$	726.71	0.88	0.80	$g_{9/2}, R=2,4$	$g_{9/2}, R=0,2$
			$\frac{7}{2}^+$	586.23	0.12	0.20		$g_{9/2}, R=2$
761.98	741	$\frac{13}{2}^+$	$\frac{9}{2}^+$	761.98	1.00	1.00	$g_{9/2}, R=2$	$g_{9/2}, R=0,2$
884.37	895	$\frac{5}{2}^-$	$\frac{5}{2}^-$	271.94	0.36	0.44	$\frac{5}{2}^-[303]$	$\frac{1}{2}^-[301]$
			$\frac{3}{2}^-$	212.94	0.31	0.17		$\frac{3}{2}^-[301]$
			$\frac{7}{2}^+$	743.8	0.16	0.02		$g_{9/2}, R=2$
			$\frac{5}{2}^+$	702.94	0.15	0.05		$g_{9/2}, R=2,4$
920.6	882	$\frac{1}{2}^+$	$\frac{5}{2}^+$	739.39	0.68	0.05	$\frac{1}{2}^+[431]$	$g_{9/2}, R=2,4$
			$\frac{1}{2}^-$	777.92	0.32	0.95		$\frac{1}{2}^-[301]$
986.18	966	$\frac{7}{2}^-$	$\frac{5}{2}^-$	373.80	0.57	0.90	$\frac{1}{2}^-[301]$	$\frac{1}{2}^-[301]$
			$\frac{5}{2}^+$	805.12	0.23	0.00		$g_{9/2}, R=2,4$
			$\frac{7}{2}^+$	845.6	0.11	0.00		$g_{9/2}, R=2$
			$\frac{3}{2}^-$	477.1	0.09	0.08		$\frac{1}{2}^-[301]$
1004.21	1005	$\frac{3}{2}^+$	$\frac{5}{2}^+$	822.98	1.0	1.0	$\frac{1}{2}^+[431]$	$g_{9/2}, R=2,4$
1019.95	1030	$^a\frac{5}{2}^+$	$\frac{7}{2}^+$	879.26	0.60	0.94	$\frac{1}{2}^+[431]$	$g_{9/2}, R=2$
			$\frac{5}{2}^+$	838.65	.0.40	0.06		$g_{9/2}, R=2,4$
1135.09	1106	$\frac{5}{2}^-$	$\frac{5}{2}^-$	522.71	0.56	0.44	$\frac{3}{2}^-[301]$	$\frac{1}{2}^-[301]$
			$\frac{5}{2}^-$	250.82	0.11	0.02		$\frac{5}{2}^-[303]$
			$\frac{3}{2}^-$	625.87	0.19	0.21		$\frac{1}{2}^-[301]$
			$\frac{5}{2}^+$	953.9	0.14	0.01		$g_{9/2}, R=2,4$
1176.55	1155	$\frac{9}{2}^-$	$\frac{5}{2}^-$	564.17	0.90	0.99	$\frac{1}{2}^-[301]$	$\frac{1}{2}^-[301]$
			$\frac{7}{2}^-$	190.6	0.10	0.01		$\frac{1}{2}^-[301]$
1203.48	1318	$\frac{9}{2}^+$	$\frac{7}{2}^+$	1062.5	0.71	0.72	$g_{9/2}, R=2,4$	$g_{9/2}, R=2$
			$\frac{9}{2}^+$	1203.48	0.29	0.12		$g_{9/2}, R=0,2$
			$\frac{11}{2}^+$	476	0.00	0.13		$g_{9/2}, R=2,4$
1207.29	1300	$\frac{7}{2}^-$	$\frac{5}{2}^-$	323.00	0.52	0.46	$\frac{5}{2}^-[303]$	$\frac{3}{2}^-[301]$
			$\frac{3}{2}^-$	535.72	0.48	0.54		$\frac{3}{2}^-[301]$
1243.95	1250	$\frac{7}{2}^+$	$\frac{5}{2}^+$	1062.72	0.57	0.36	$\frac{1}{2}^+[431]$	$g_{9/2}, R=2,4$
			$\frac{7}{2}^+$	1103.1	0.11	0.18		$g_{9/2}, R=2$
			$\frac{9}{2}^+$	1243.4	0.32	0.46		$g_{9/2}, R=0,2$
1306.43	1427	$\frac{7}{2}^+$	$\frac{5}{2}^+$	1128.4	0.82	0.74	$g_{9/2}, R=2,4$	$g_{9/2}, R=2,4$
			$\frac{7}{2}^+$	1168.2	0.18	0.24		$g_{9/2}, R=2$
1329.52	1405	$\frac{7}{2}^-$	$\frac{7}{2}^+$	1188.94	0.52	0.20	$\frac{3}{2}^-[301]$	$g_{9/2}, R=2$
			$\frac{5}{2}^-$	716.97	0.48	0.48		$\frac{1}{2}^-[301]$
1444.23	1414	$^a\frac{3}{2}^+$	$\frac{5}{2}^+$	1262.99	0.54	0.84	$g_{9/2}, R=2,4$	$g_{9/2}, R=2,4$
			$\frac{7}{2}^+$	1304	0.00	0.16		$g_{9/2}, R=2$
			$\frac{3}{2}^-$	935.2	0.25	0.00		$\frac{1}{2}^-[301]$
			$\frac{5}{2}^-$	832.2	0.21	0.00		$\frac{1}{2}^-[301]$
1526.46	1558	$\frac{15}{2}^+$	$\frac{13}{2}^+$	764.48	0.67	0.42	$g_{9/2}, R=4$	$g_{9/2}, R=2$

TABLE V. (*Continued*).

E_i (keV)		I_i^π	I_f^π	E_γ (keV)	Branching ratio		Theoretical identification	
Expt.	Theor.				Expt.	Theor.	Initial state	Final state
			$\frac{11}{2}^+$	799.74	0.33	0.58		$g_{9/2}, R=2,4$
1552.59	1771	$(\frac{7}{2}^+)$	$\frac{5}{2}^+$	1371.36	0.63	0.52	$g_{9/2}, R=4$	$g_{9/2}, R=2,4$
			$\frac{7}{2}^+$	1412.2	0.37	0.21		$g_{9/2}, R=4$
1585.02	1576	$(\frac{17}{2}^+)$	$\frac{13}{2}^+$	823.04	1.00	1.00	$g_{9/2}, R=4$	$g_9 2, R=2$
1604.91	1597	$(\frac{11}{2}^-)$	$\frac{7}{2}^-$	618.73	1.00	0.76	$\frac{1}{2}^-[301]$	$\frac{1}{2}^-[301]$
			$\frac{9}{2}^-$	428	0	0.770		$\frac{1}{2}^-[301]$
1747.45	1800	$\frac{13}{2}^-$	$\frac{9}{2}^-$	570.90	1.00	1.00	$\frac{1}{2}^-[301]$	$\frac{1}{2}^-[301]$

[a]Other spins are allowed experimentally.

function of N. For pure Nilsson bands, with no Coriolis mixing, transition probabilities for interband $M1$ transitions between the $3/2^-[301]$ and $1/2^-[301]$ bands would be very large since they are spin-flip transitions, typically 20–100 times larger than calculated probabilities of intraband transitions in pure $3/2^-[301]$ and $5/2^-[303]$ bands. Thus when the Coriolis interaction mixes $1/2^-[301]$ and $3/2^-[301]$ components into the $5/2^-[303]$ band, excited members of the $5/2^-$ band decay predominantly through interband transitions rather than intraband transitions. In ^{97}Tc and ^{99}Tc, only interband transitions were observed, while in ^{101}Tc interband and intraband transitions were observed with roughly equal intensities. This argues for a decrease in Coriolis mixing as a result of an increase in deformation.

Perhaps the most dramatic systematic evidence for the change in deformation can be found in the order of the lowest-lying positive-parity states. From the Nilsson diagram of Fig. 5, one would expect members of the $5/2^+[422]$ band to lie at low excitation energies. Indeed this is the case, in that the lowest states are $5/2^+$, $7/2^+$, and $9/2^+$. But in the lighter isotopes, the Coriolis interaction has inverted the order of these states. Figure 8 illustrates the systematics. The horizontal axis represents the strength of the Coriolis interaction. No units are given, because it is not linear with respect to N. The upper portion of Fig. 8 shows calculated energies, where parameters have been chosen that best reflect the entire set of positive-parity states in the appropriate Tc isotopes, not just the lowest three. The vertical scale is energy, but the figure shows the $5/2^+$ state at the same energy in all cases. If the strength of the Coriolis interaction were zero, the calculation would yield a regular rotational band. The left-most calculation is close to this limit. The bottom portion of the figure shows energies of experimental states in ^{103}Tc, ^{101}Tc, ^{99}Tc, ^{97}Tc, and ^{95}Tc. The overall systematic correspondence to the theoretical energies is clear.

VI. CONCLUSIONS

The present work has extended previously available information on the properties of intermediate-spin states in the low-energy region of ^{99}Tc. The ^{98}Mo(^{3}He,$pn\gamma$)^{99}Tc reaction has proven to be effective in populating both yrast and non-yrast states. Thirty-five new levels have been established, which roughly doubles the number of known states below 2 MeV. The use of the proton-γ coincidence system, by reducing background and eliminating photopeaks from competing reaction channels, allowed the quantitative analysis of many weak transitions placed in the level scheme. As a result reliable spin assignments could be established for the majority of states.

The interpretation of the structure of ^{99}Tc in the framework of a rotational model has proven to be successful. Four reasonably pure rotational bands have been identified in ^{99}Tc, based on $1/2^-[301]$, $3/2^-[301]$, $5/2^-[303]$, and $1/2^+[431]$ Nilsson states. Coriolis mixing is smallest for the three negative-parity bands identified, and although somewhat larger in the positive-parity band identified, is still small enough to retain its nature as a $1/2^+[431]$ rotational band.

Positive-parity states for which $g_{9/2}$ parentage is deduced exhibit a larger degree of Coriolis mixing. There is no consistent band structure for these states. However, many of the lowest-lying states have a large component of a single Nilsson state. For example, the lowest $5/2^+$ state is 44% $5/2^+[422]$.

The deduced results for ^{99}Tc fit naturally into systematics which argue for an increase in deformation as a function of neutron number going from ^{95}Tc to ^{103}Tc.

ACKNOWLEDGMENT

This work was supported in part by the National Science Foundation.

[1] C. S. Whistnant, K. D. Carnes, R. H. Castain, F. A. Rickey, G. S. Samudra, and P. C. Simms, Phys. Rev. C **34**, 443 (1986).

[2] Sadek Zeghib, F. A. Rickey, G. S. Samudra, P. C. Simms, and Ning Wang, Phys. Rev. C **36**, 939 (1987).

[3] Hurol Aslan, Ben Crowe, Tim Dague, D. G. Savage, Sadek Zeghib, F. A. Rickey, and P. C. Simms, Phys. Rev. C **54**, 576 (1996).

[4] D. G. Savage, Hurol Aslan, Ben Crowe, Tim Dague, Sadek Zeghib, F. A. Rickey, and P. C. Simms, Phys. Rev. C **55**, 120 (1997).

[5] H. A. Smith, Jr. and F. A. Rickey, Phys. Rev. C **14**, 1946 (1976).
[6] H. W. Muller and D. Chnielewska, Nucl. Data Sheets **48**, 663 (1986).
[7] H. C. Cheung, S. I. Hayakawa, J. E. Kitching, J. K. P. Lee, S. K. Mark, and J. C. Waddington, Z. Phys. A **280**, 149 (1977).
[8] K. Singh and H. S. Sahota, J. Phys. Soc. Jpn. **51**, 3766 (1982).
[9] K. O. Zell, H. Harter, D. Hippe, H. W. Schuh, and P. von Bretano, Z. Phys. A **316**, 351 (1984).
[10] W. Zipper, A. Dewald, W. Lieberz, R. Reinhardt, W. Dichter, F. Seiffert, and P. von Brentano, Nucl. Phys. **A504**, 36 (1989).
[11] Jean Kern, Pavel Cejnar, and Wiktor Zipper, Nucl. Phys. **A554**, 246 (1993).
[12] K. S. Krane, R. M. Steffen, and R. M. Wheeler, Nucl. Data, Sect. A **11**, 351 (1973).
[13] J. A. Grau, L. E. Samuelson, F. A. Rickey, P. C. Simms, and H. A. Smith, Phys. Rev. C **14**, 2297 (1976).
[14] *Interacting Bose-Fermion Systems in Nuclei*, edited by F. Iachello (Plenum, New York, 1981).
[15] S. G. Nilsson, K. Dan. Vidensk. Selsk. Mat. Fys. Medd. **29**, No. 16 (1955).
[16] Rakesh Popli, J. A. Grau, S. I. Popik, L. E. Samuelson, F. A. Rickey, and P. C. Simms, Phys. Rev. C **20**, 1350 (1979).
[17] M. A. J. Mariscotti, G. Scharff-Goldhaber, and B. Buck, Phys. Rev. **178**, 1864 (1969).
[18] B. Reehal and R. Sorenson, Phys. Rev. C **2**, 819 (1970).
[19] Balraj Singh, Nucl. Data Sheets **67**, 693 (1992).
[20] P. Luksch, Nucl. Data Sheets **38**, 1 (1983).
[21] B. A. Brown, A. Etchegoyan, and W. D. M. Rae, Computer Code OXBASH, MSU-NSCL Report No. 524.
[22] Jean Blachot, Nucl. Data Sheets **68**, 311 (1993).